Sensitivity of a Cumulus Parameterization Scheme to Precipitation Production Representation and Its Impact on a Heavy Rain Event over Korea

JI-YOUNG HAN AND SONG-YOU HONG

Korea Institute of Atmospheric Prediction Systems, Seoul, South Korea

KYO-SUN SUNNY LIM

Pacific Northwest National Laboratory, Richland, Washington

JONGIL HAN

Systems Research Group, Inc. and National Centers for Environmental Prediction/Environmental Modeling Center, Camp Springs, Maryland

(Manuscript received 27 July 2015, in final form 16 March 2016)

ABSTRACT

The sensitivity of a cumulus parameterization scheme (CPS) to a representation of precipitation production is examined. To do this, the parameter that determines the fraction of cloud condensate converted to precipitation in the simplified Arakawa–Schubert (SAS) convection scheme is modified following the results from a cloud-resolving simulation. While the original conversion parameter is assumed to be constant, the revised parameter includes a temperature dependency above the freezing level, which leads to less production of frozen precipitating condensate with height. The revised CPS has been evaluated for a heavy rainfall event over Korea as well as medium-range forecasts using the Global/Regional Integrated Model system (GRIMs). The inefficient conversion of cloud condensate to convective precipitation at colder temperatures generally leads to a decrease in precipitation, especially in the category of heavy rainfall. The resultant increase of detrained moisture induces moistening and cooling at the top of clouds. A statistical evaluation of the medium-range forecasts with the revised precipitation conversion parameter shows an overall improvement of the forecast skill in precipitation and large-scale fields, indicating importance of more realistic representation of microphysical processes in CPSs.

1. Introduction

Cumulus convection has a major impact not only on the hydrological cycle through precipitation but also on the large-scale flow by the release of latent heat and vertical transport of sensible heat, water vapor, and momentum. Therefore, an understanding of the interaction of cumulus convection with the large-scale environment and its adequate parameterization in atmospheric modeling is crucial for improved weather and climate prediction. Considerable efforts have been devoted to the improvement of cumulus parameterization since numerical weather prediction (NWP) models were introduced in the 1960s. However, there are still many simplifications and assumptions that should be improved in the parameterized convective processes. In particular, microphysical processes for convective clouds are generally parameterized in an overly simplified manner with crude assumptions, especially in global NWP models.

It is assumed in most convective microphysics parameterizations that a portion of condensed water is converted into precipitation with an empirically chosen constant conversion rate (e.g., Tiedtke 1989; Zhang and McFarlane 1995; Han and Pan 2011). By performing sensitivity experiments with the Arakawa and Schubert (1974) convection scheme, Lord (1978) indicated that the vertical distribution of condensed water is quite sensitive to the conversion parameter, but the predicted precipitation rate is insensitive to it. However, Segele et al. (2009) showed that the parameter that determines the amount of condensed water that ultimately falls out

Corresponding author address: Ji-Young Han, Korea Institute of Atmospheric Prediction Systems, 4F, Hankuk Computer Building, 35 Boramae-Ro 5 Gil, Dongjak-Gu, Seoul 07071, South Korea.
E-mail: jy.han@kiaps.org

DOI: 10.1175/MWR-D-15-0255.1

as rain crucially affects the simulated precipitation amount over the Horn of Africa in a regional climate model simulation with the Emanuel (1991) convection scheme. Using a global climate model with the Zhang and McFarlane (1995) convection scheme, recent studies have shown that the conversion parameter over the ocean has a strong impact on the cloud water path and cloud and radiation properties (Yang et al. 2013), and a decrease in this parameter is most effective in improving the Madden–Julian oscillation (MJO) simulation (Boyle et al. 2015). Song et al. (2012) implemented sophisticated microphysical processes from cloud microphysics scheme in the Zhang and McFarlane scheme and showed that a proper representation of convective microphysical processes in a global climate model is important for reliable climate simulation.

In this study, we investigate the sensitivity of a cumulus parameterization scheme (CPS) to the precipitation production term and its impact on simulated precipitation and large-scale fields by using a revised form of the conversion parameter, which is derived from the cloud-resolving simulation results. For this, we perform an experiment for a heavy rainfall event over the Korean Peninsula and medium-range forecast experiments using a global atmospheric model. The model used in this study, a revised cloud microphysical process in a CPS, and experimental design are described in section 2. The results with the revised conversion parameter are presented in section 3. A summary and conclusions are given in section 4.

2. Model and experimental setup

a. Model description

The global atmospheric model used in this study is the Global/Regional Integrated Model system (GRIMs) global model program (GMP) with the spherical harmonics dynamical core (Hong et al. 2013). The GRIMs is a multiscale atmospheric model system with unified physics that has been developed for NWP, seasonal simulations, and climate research projects from global to regional scales. The physics parameterization schemes employed in this study include the Rapid Radiative Transfer Model for general circulation models (RRTMG; Iacono et al. 2008), the Weather Research and Forecasting (WRF) single-moment 5-class (WSM5) microphysics scheme (Hong et al. 2004), the simplified Arakawa–Schubert (SAS) deep convection scheme (Pan and Wu 1995; Hong and Pan 1998; Lim et al. 2014), the GRIMs shallow convection scheme (Hong et al. 2012), the diagnostic cloudiness scheme (Hong et al. 1998; Ham et al. 2009), the Yonsei University (YSU) boundary layer scheme (Hong et al. 2006) with enhanced stable boundary layer mixing (Hong 2010), the Noah land surface model (Ek et al. 2003), the ocean mixed layer model (Kim and Hong 2010), and the orographic and convective gravity wave drag parameterization schemes proposed by Kim and Arakawa (1995) and Chun and Baik (1998), respectively. The model uses the National Centers for Environmental Prediction (NCEP) Global Forecast System (GFS) Final (FNL) analysis data and the observed sea surface temperature (SST) and snow data as initial atmospheric and surface boundary conditions, respectively. The model has 64 hybrid sigma–pressure vertical levels and a model top at 0.3 hPa.

b. SAS convection scheme

The original Arakawa and Schubert (1974) convection scheme was simplified by Grell (1993) with a saturated downdraft by considering only a single updraft–downdraft couplet within a single grid cell, thus leading to the SAS scheme. Subsequent modifications have been made to this scheme (Hong and Pan 1998; Lim et al. 2014) after its first implementation in the NCEP Medium-Range Forecast model in 1993 (Pan and Wu 1995). The SAS scheme uses a mass-flux concept to adjust the atmospheric temperature and moisture fields. The cloud-base mass flux is determined using a quasi-equilibrium assumption that the destabilization of an air column by the large-scale forcing is nearly balanced by the stabilization by the cumulus convection. The degree of moist convective instability is determined by the cloud work function, which is a measure of the integrated cloud buoyancy (including the water-loading effect due to cloud condensates). The cloud work function must be larger than zero for convection to be initiated. The feedback of the convection on the large-scale environment occurs through the mass flux in the subsidence, entrainment–detrainment process, and cloud microphysical processes. Since detailed formulation of the SAS scheme is described in Pan and Wu (1995) and Park and Hong (2007), here only a revised cloud microphysical process is described.

The precipitation rate due to the cumulus updraft–downdraft couplet for each cloud layer k in the SAS scheme is given by

$$\Delta R(k) = m_u(k+1/2)C_0\Delta z(k)\Delta q_l(k) - m_d(k+1/2)\Delta q_e(k), \quad (1)$$

where m_u and m_d are the updraft and downdraft mass fluxes, respectively; C_0 is the conversion parameter that determines the fraction of condensate that is converted to precipitation; Δz is the thickness of layer; Δq_l is the

amount of condensate; and Δq_e is the amount of moisture that is necessary to keep the downdraft saturated. In the original SAS convection scheme, a portion of cloud condensate is converted into precipitation by assuming a constant conversion rate per unit height. Then the amount of precipitation over a time step Δt is calculated using

$$R = \sum_k \Delta R(k)\Delta t. \tag{2}$$

To evaluate the sensitivity to precipitation production in a CPS, a revised conversion parameter for convective precipitation that is proposed based on the results from a three-dimensional (3D) cloud-resolving simulation of a convective storm (Lim 2011) is used. The cloud-resolving simulations were performed using the WRF double-moment 6-class (WDM6) bulk microphysics scheme with various aerosol concentrations under different environmental moisture conditions. Analyzed results show that the ratio of the amount of precipitating condensates (rain, snow, and graupel) to the amount of nonprecipitating condensates (cloud liquid water and ice) decreases exponentially with height above the freezing level (Fig. 1), indicating less production of frozen precipitating condensates with height. Based on this result, the conversion parameter (C_0) is modified to take the form of an exponential function of temperature below the freezing temperature so that the fraction of cloud ice that is converted to precipitation decreases with height above the freezing level, whereas the value for warm microphysics keeps constant:

$$C_0(z) = a\exp\{b[T(z) - T_0]\} \quad \text{for} \quad T \le T_0, \tag{3a}$$

$$C_0(z) = a \quad \text{for} \quad T > T_0, \tag{3b}$$

where a ($=2.0 \times 10^{-3}\,\mathrm{m}^{-1}$) is a constant, and b ($=0.07^{\circ}\mathrm{C}^{-1}$) is the exponential decaying rate of C_0 below the freezing temperature T_0 ($=0^{\circ}$C). Note that C_0 for temperatures above T_0 is equal to the value in the original SAS scheme. The formula of Eq. (3a) mimics the ice microphysics of Fletcher (1962) having abundant ice nuclei at colder temperatures. It is also noted that aggregation and accretion in the ice processes proceed most rapidly in the cloud layer at temperatures between -10° and 0°C, and most of the precipitation growth occurs in this lower cloud layer (Braham 1968; Rogers and Yau 1988).

Uncertainty exists in deriving the ratio from a full 3D cloud-resolving simulation result since this derived ratio is applied only to the updrafts in a CPS. To alleviate this uncertainty, the ratio of precipitation over cloud condensates in a cloud-resolving simulation is obtained by averaging them over the precipitation core during the mature stage. Also, revised property in conversion parameter is applied only above the freezing level where convective updrafts are dominant. Note that the exponential decrease of the ratio is also seen in an idealized 2D squall-line simulation by Lim and Hong (2012) (not shown). Although the ratio of precipitating to nonprecipitating condensates from a cloud-resolving simulation cannot provide a conclusive form of the bulk conversion rate for a CPS due to multiple pathways that can also affect this ratio in the cloud-resolving model, we believe that the proposed conversion ratio is more realistic than a constant value in the original SAS scheme.

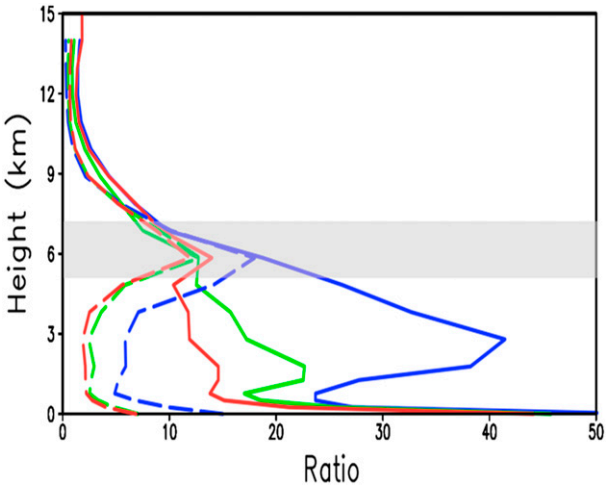

FIG. 1. Ratio of the amount of precipitating condensates (rain, snow, and graupel) to the amount of nonprecipitating condensates (cloud liquid water and ice) obtained from a cloud-resolving simulation of a convective storm with various aerosol concentrations under different environmental moisture conditions conducted by Lim (2011). The blue, green, and red lines correspond to the experiments with maritime-, continental-, and extreme continental-type aerosols, respectively. The solid and dashed lines correspond to the experiments under moist and dry environments, respectively. The layer at temperatures between -10° and 0°C is represented by the gray shaded region.

A temperature dependency for the conversion of cloud ice to convective precipitation was also considered by Emanuel and Živković-Rothman (1999). They allowed the autoconversion threshold to be temperature dependent above the freezing level. However, in contrast to our study, the autoconversion threshold in their study decreases linearly with decreasing temperature above the freezing level, which leads to efficient conversion at colder temperatures. Their parameterization is against the fact that aggregation and accretion in the ice processes (precipitation growth processes) proceed most rapidly in the lower cloud layer. Meanwhile, Nober et al. (2003) introduced the formation of raindrops

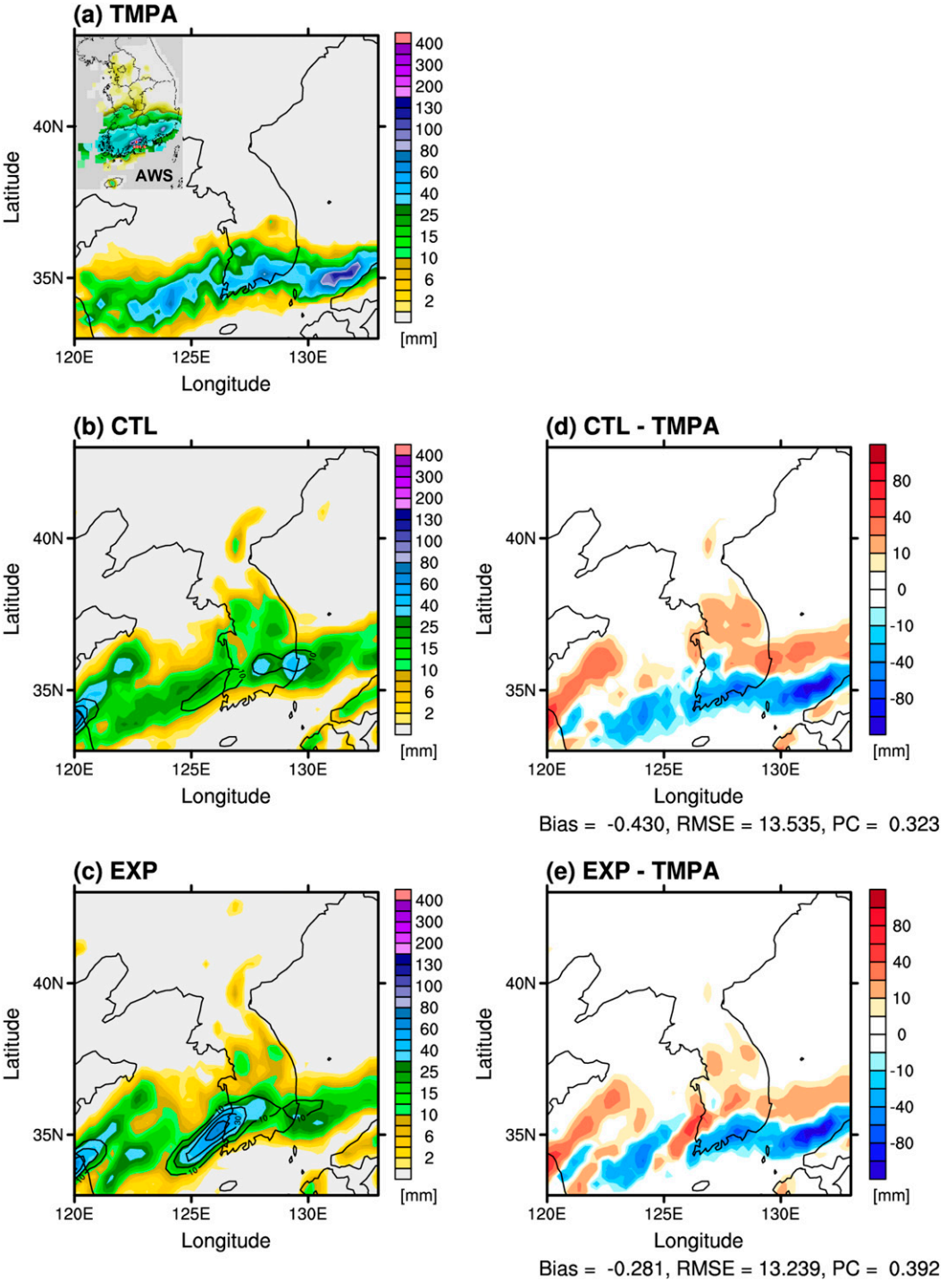

FIG. 2. Spatial distribution of the 12-h accumulated precipitation amount (mm) at 0600 UTC 7 Jul 2013 obtained from the (a) TMPA observation and AWS rain gauge observations over South Korea [inset in (a)] and the simulation results from (b) CTL and (c) EXP, and the differences (d) between CTL and TMPA and (e) between EXP and TMPA. The contour lines in Figs. 2b and 2c indicate the amount of grid-scale precipitation. The mean bias, RMSE, and pattern correlation are shown at the bottom of Figs. 2d and 2e.

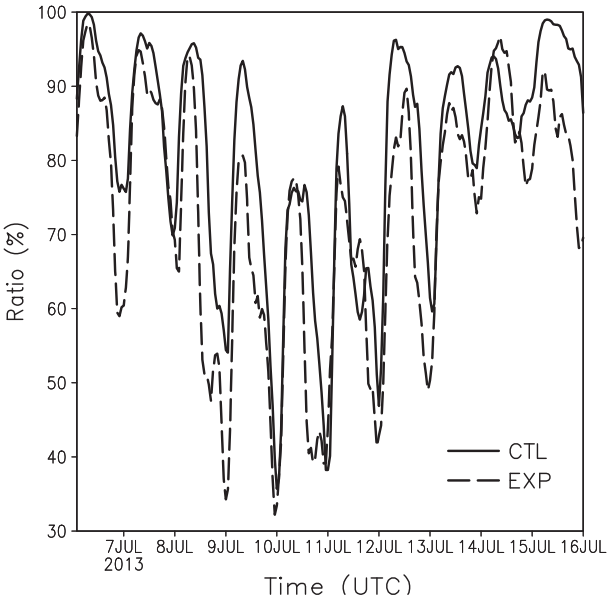

FIG. 3. Time series of the ratio of convective to total precipitation averaged over East Asia (25°–50°N, 105°–145°E) from CTL (solid) and EXP (dashed).

depending on cloud droplet number concentration and temperature based on satellite observations, but only for warm rain processes (i.e., conversion of cloud droplets to raindrops).

c. *Experimental design*

To understand the sensitivity of a CPS to the variation of precipitation production and its impacts on simulated precipitation and large-scale fields, we perform experiments for a heavy rainfall event over the Korean Peninsula on 7 July 2013 and medium-range forecast experiments during the period of July 2013 with both original and revised conversion parameters. The heavy rainfall event considered in this study occurred over the southern part of the Korean Peninsula along the Changma front on 7 July 2013 (see Fig. 2a), and a maximum rainfall of over 100 mm was recorded in the southern coastal areas of Korea from 1800 UTC 6 July to 0600 UTC 7 July 2013 by the rain gauge. The experiment is integrated for 10 days starting from 0000 UTC 6 July 2013 at T510 (~25 km) horizontal resolution. For the statistical evaluation of the medium-range forecasts, 10-day forecasts initiated at every 0000 UTC from 1 to 31 July 2013, which is within the East Asian summer monsoon period, are also performed at T254 (~50 km) horizontal resolution. In the following section, the control experiment with the original SAS convection scheme (i.e., with constant C_0) is referred to as CTL, and the experiment with the C_0 of Eq. (3) is referred to as EXP.

3. Results and discussion

The sensitivity to conversion parameter is mainly discussed through a case study for a heavy rainfall event over Korea. Then the performance is statistically evaluated using medium-range forecast experiments with particular focus on the forecast skill over East Asia, including South Korea, which is the region of interest in this study.

a. *Heavy rainfall event over Korea on 7 July 2013*

Figures 2a–c show the spatial distribution of the 12-h accumulated precipitation amount at 0600 UTC 7 July 2013 obtained from the Tropical Rainfall Measuring Mission (TRMM) Multisatellite Precipitation Analysis (TMPA) observation and automatic weather station

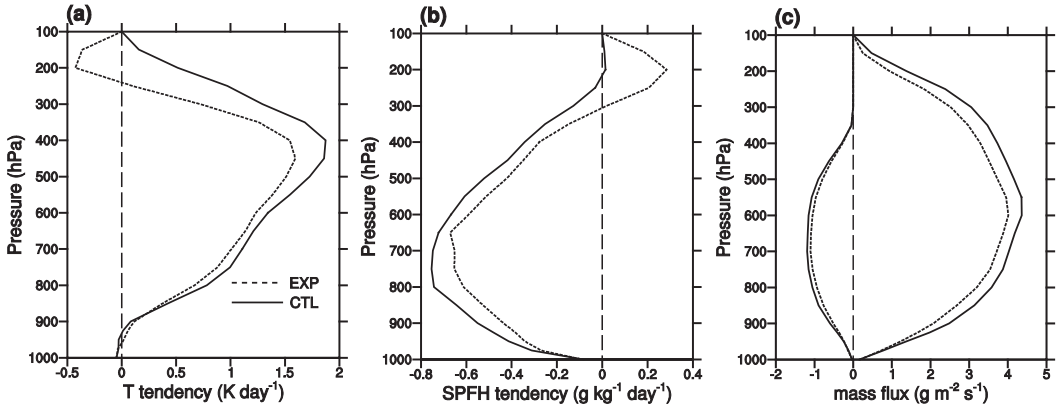

FIG. 4. Vertical profiles of the tendency of (a) temperature (K day^{-1}) and (b) specific humidity (g kg^{-1} day^{-1}) due to deep convection and (c) the updraft and downdraft mass fluxes (g m^{-2} s^{-1}) averaged over East Asia and 5-day forecast period from CTL (solid) and EXP (dashed).

TABLE 1. High, middle, and low cloud fraction (%) and cloud work function (J kg^{-1}) averaged over East Asia and 5-day forecast period from CTL and EXP. The values of the cloud work function in parentheses are those calculated without considering the water-loading effect due to cloud condensate.

	CTL	EXP
High cloud fraction	31.3	41.3
Middle cloud fraction	17.3	23.3
Low cloud fraction	27.6	28.7
Cloud work function	36.9 (39.8)	30.4 (35.4)

(AWS) rain gauge observations over South Korea and the simulation results from CTL and EXP. Both CTL and EXP reproduce the overall distribution of rainfall over Korea: an east–west-oriented precipitation band along the Changma front in the southern part of the Korean Peninsula. However, the location of the band is shifted northward in comparison with the observation, and its amount is underestimated. Although not seen in the TMPA product, relatively weak precipitation (12-h accumulated precipitation amount less than 10 mm) was recorded in the middle part of the peninsula by the rain gauge. The amount of precipitation in that region is overestimated in CTL, but in EXP it is significantly reduced and in better agreement with the rain gauge observations. Note that the mean bias, root-mean-square error (RMSE), and pattern correlation of the precipitation against the TMPA observation are improved in EXP compared to those in CTL (Figs. 2d,e). It is found that EXP generally tends to decrease precipitation by suppressing conversion of cloud condensate to convective precipitation at colder temperatures. However, in some regions, for example, in the Yellow Sea, southwest of Korea, total precipitation is increased in EXP due to increased grid-scale precipitation.

Figure 3 depicts the time series of the ratio of convective to total precipitation averaged over East Asia (25°–50°N, 105°–145°E) from both experiments. The ratio of convective to total precipitation reveals a diurnal variation with its maximum in the afternoon and minimum in the early morning. As expected, the ratio in EXP is smaller than that in CTL because the inefficient conversion of cloud condensate to convective precipitation at colder temperatures results in suppressed convective precipitation. On the other hand, grid-scale precipitation is found to be larger than that from CTL. This is because the reduced conversion rate to convective precipitation increases the detrainment of moisture from cumulus convection, which in turn increases grid-scale precipitation. Because in the current CPS the decrease in convective precipitation is generally greater than the increase in grid-scale precipitation, total precipitation in EXP is on average smaller than CTL (e.g., 12-h accumulated precipitation amounts at 0600 UTC 7 July 2013 averaged over East Asia are approximately 2.4 and 1.9 mm in CTL and EXP, respectively).

TABLE 2. Shortwave (SW), longwave (LW), and net (SW + LW) radiation fluxes (W m^{-2}; positive means downward) at the top of atmosphere (TOA) and surface (SFC) averaged over East Asia and 5-day forecast period from CTL. The values in parentheses are those from EXP.

	SW	LW	Net
TOA	358 (341)	−261 (−247)	97 (94)
SFC	251 (235)	−55 (−52)	196 (183)

It is seen that CTL produces enhanced heating and drying throughout the troposphere by cumulus-induced subsidence and very weak moistening at the top of clouds (Figs. 4a,b). In EXP, convective heating and drying is decreased throughout the troposphere, except below 900 hPa where downdraft cooling is also reduced. This reduced convective activity is confirmed by the reduction of mass fluxes (Fig. 4c), and by the reduction of buoyancy (see cloud work function in Table 1). This weakened convection in EXP can be explained by the water-loading effect in updrafts and interaction with other processes. It is clear from Table 1 that EXP produces a larger cloud fraction compared to CTL, especially in the mid- to upper troposphere, due to enhanced moisture detrainment. The increase of cloudiness reduces the net shortwave radiation flux at the surface by reflecting more incoming solar radiation and increases the net longwave radiation flux by trapping more outgoing longwave radiation (Table 2). Because the relative cooling due to reduced shortwave effect surpasses the heating due to weakened longwave effect, the air column becomes less convectively buoyant, as evidenced by the decrease in the cloud work function (a measure of the integrated cloud buoyancy) in Table 1. Given the amount of updraft mass flux, the reduced conversion to precipitation can induce the increase of cloud water loading. Further reduction of buoyancy in the presence of the water-loading effect confirms the enhanced loading in EXP (Table 1). Note that only the longwave effect exists at nighttime. It is confirmed that the difference in the cloud buoyancy between the two experiments becomes small at night because the cloud longwave effect and the water-loading effect compensate each other (not shown). The decrease of heating and drying is more pronounced in the upper troposphere. This is because the increase of detrained moisture with the revised scheme results in stronger cooling and moistening at the top of clouds. Note that both CTL and EXP have moisture detrainment near the cloud top. However, in CTL, the amount of detrainment is too small to induce cooling due to efficient conversion to falling

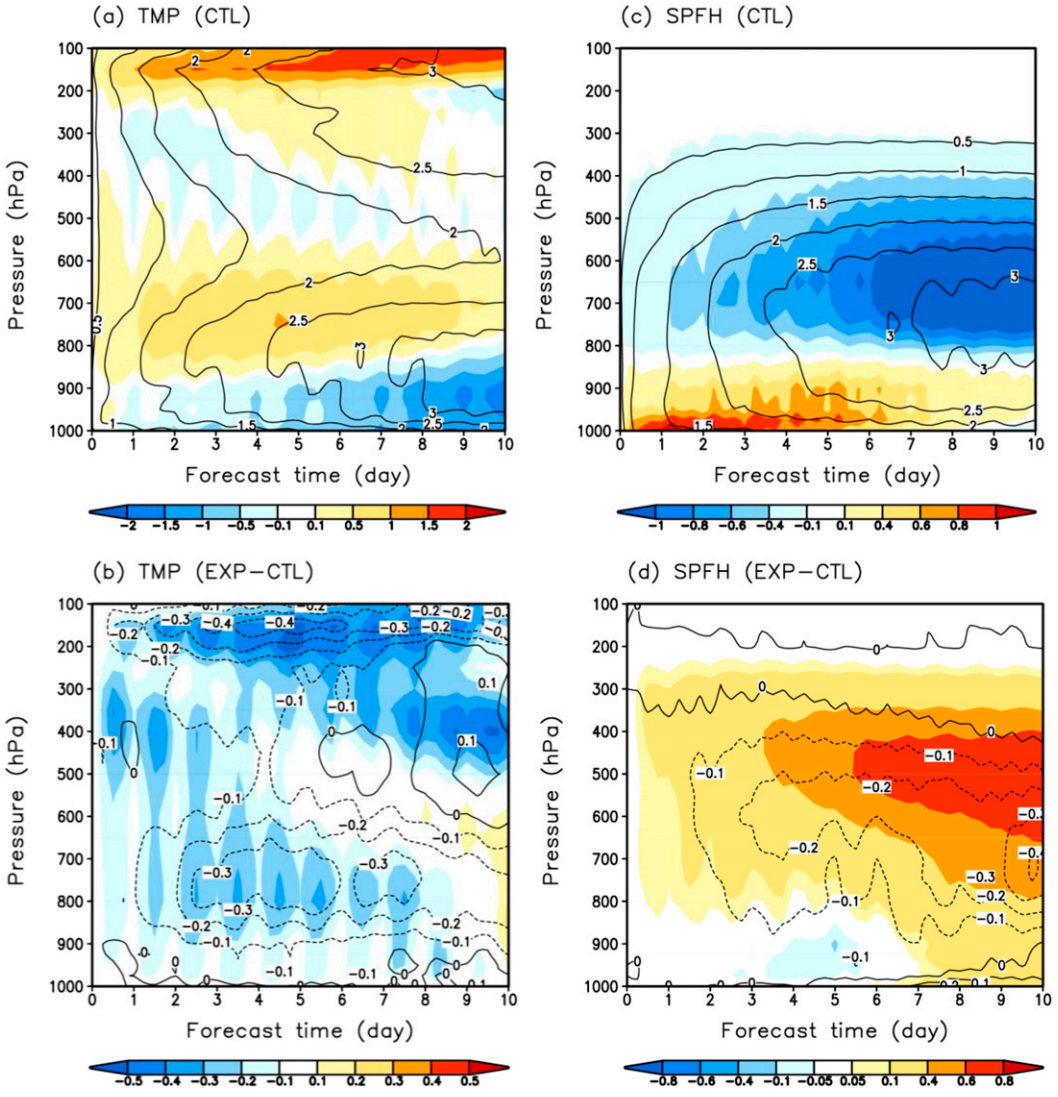

FIG. 5. Time series of the vertical profiles of the biases (shaded) and RMSEs (contour) of (a),(b) temperature (K) and (c),(d) specific humidity (g kg^{-1}) against the NCEP GFS FNL analysis data during the period of July 2013 averaged over East Asia from (top) CTL and (bottom) the difference between EXP and CTL.

precipitation, whereas the amount of detrained moisture is enough to induce cooling in EXP.

b. *Statistical evaluation of the medium-range forecasts for July 2013*

Figure 5 shows the time series of the vertical profiles of the biases and RMSEs of temperature and specific humidity against the NCEP GFS FNL analysis data during the period of July 2013 averaged over East Asia from CTL and the difference between EXP and CTL. CTL has an overall warm and dry bias above 850 hPa and a cold and wet bias below the level (Figs. 5a,c). It is apparent from Figs. 5b and 5d that the biases and RMSEs of temperature and specific humidity are significantly alleviated in EXP, although there are some layers where the biases and RMSEs are slightly increased (e.g., lower troposphere after forecast day 7). A significant reduction in the warm and dry bias above the lower troposphere in EXP is attributable to the reduced heating and drying resulting from suppressed convection and the cooling and moistening due to enhanced detrainment at the top of clouds.

To statistically evaluate the performance of the revised conversion parameter for convective precipitation, various standard skill scores such as the equitable threat score (ETS) and bias score for precipitation (Fig. 6), the RMSEs for large-scale variables (Fig. 7a and Table 3), and the anomaly correlation (AC) for the 500-hPa

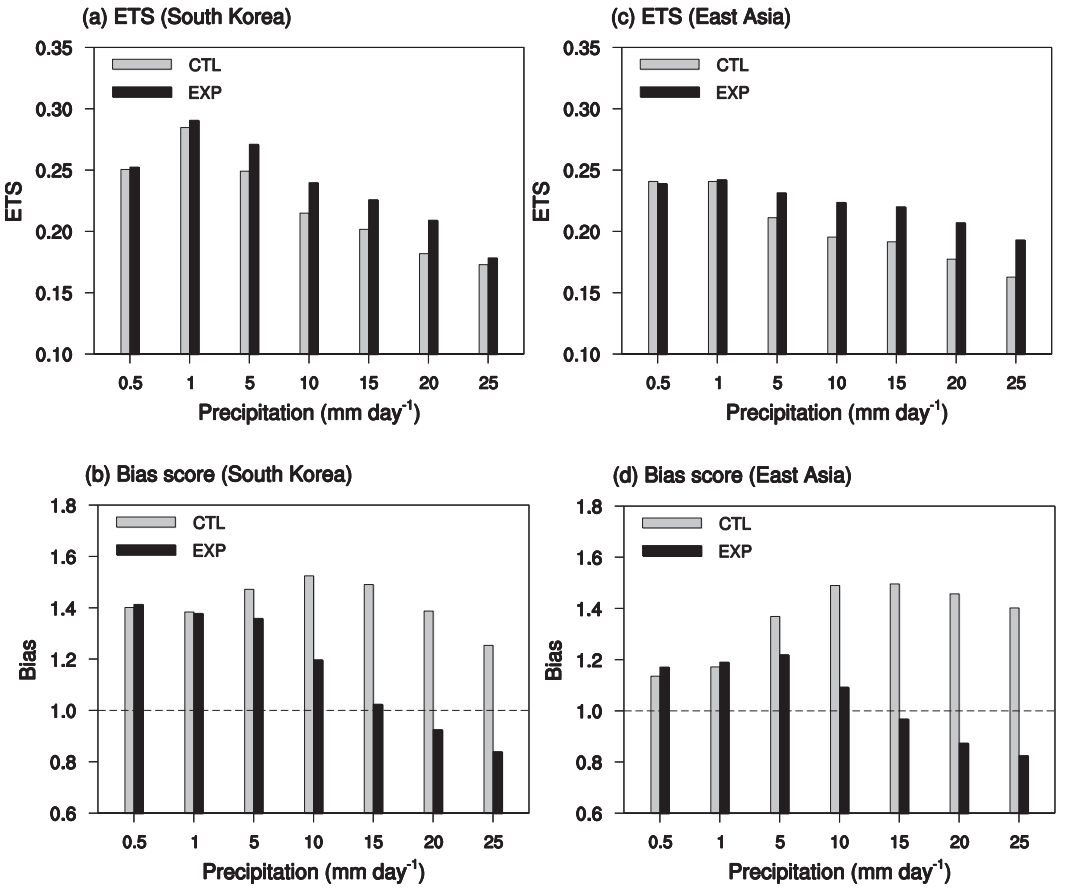

FIG. 6. (top) ETS and (bottom) bias score for precipitation forecasts from CTL (gray) and EXP (black) for forecast day 2 during the period of July 2013 (a),(b) over South Korea (33°06′–38°45′N, 124°53′–131°52′E) against AWS rain gauge observations and (c),(d) over East Asia (25°–50°N, 105°–145°E) against the CPC unified gauge-based precipitation analysis.

geopotential height (Fig. 7b) are calculated for the two medium-range forecast experiments. Note that a higher ETS and a bias score close to 1 indicate better precipitation forecast skill. The ETS for precipitation forecasts over South Korea against AWS rain gauge observations is higher in EXP than in CTL for all precipitation thresholds considered (Fig. 6a). While a higher ETS is observed for all forecast days from 2 to 5, the ETS from EXP is slightly lower than that from CTL for light precipitation with thresholds of 0.5 and 1 mm day^{-1} for forecast day 1 (not shown). It is evident from Fig. 6b that CTL tends to overestimate rainfall over South Korea for all precipitation categories. In addition, the increase of bias with the forecast time is pronounced in the categories larger than 5 mm day^{-1} (not shown). EXP in general has a better bias score than CTL by alleviating the existing systematic bias of overestimated precipitation in CTL. Although EXP tends to underestimate rainfall for heavier precipitation categories, the bias is smaller than CTL. The difference in the bias score between the two experiments for light precipitation below 1 mm day^{-1} is very small compared to that for the moderate to heavy precipitation categories, which may be because there is almost no change in the conversion parameter for convective precipitation in the case of low clouds that usually produce light precipitation. The skill of predicted precipitation over East Asia against the Climate Prediction Center (CPC) unified gauge-based precipitation analysis (Figs. 6c,d) shows a similar behavior with that over South Korea; that is, a higher ETS and a better bias score in EXP by alleviating the systematic bias of excessive precipitation in the original scheme but underestimation of heavy precipitation. The skill improvement over the globe in EXP generally follows the scores in Fig. 6 (not shown).

A statistical evaluation of large-scale fields against the NCEP GFS FNL analysis data shows an overall improvement of the medium-range forecast skill in EXP. Compared to CTL, for example, the RMSE and AC for forecasts of the 500-hPa geopotential height are improved with the revised conversion parameter in the

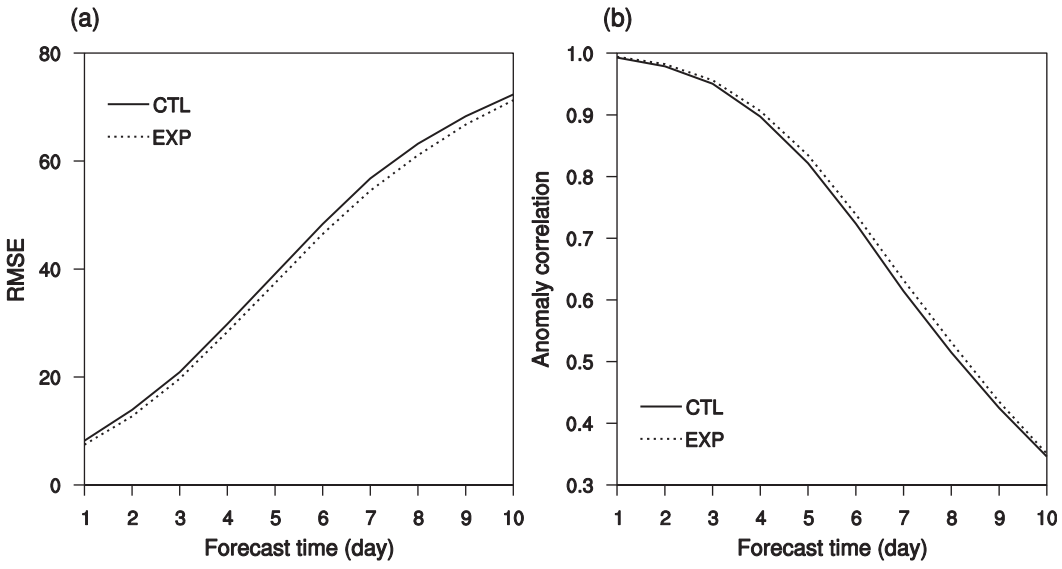

FIG. 7. (a) RMSE and (b) AC for forecasts of the 500-hPa geopotential height in the Northern Hemisphere (20°–90°N) against the NCEP GFS FNL analysis data during the period of July 2013.

Northern Hemisphere (20°–90°N) throughout the 10-day forecast period (Fig. 7). The RMSEs for large-scale variables are all reduced in the Northern Hemisphere and comparable in the Southern Hemisphere (20°–90°S) (Table 3). In the tropics (20°S–20°N), the skill for forecasts of the wind vector is better at 250 and 850 hPa and comparable at 500 hPa.

4. Summary and conclusions

In this study, the sensitivity of a CPS to a representation of precipitation production is examined. To do this, the parameter that determines the fraction of condensate that is converted to precipitation in the SAS convection scheme is modified to include a temperature dependency based on the results from a cloud-resolving simulation of a convective storm. While the original conversion parameter is assumed to be constant, the revised one decreases exponentially with decreasing temperature above the freezing level, which leads to less production of frozen precipitating condensate with height. We perform an experiment for a heavy rainfall event over Korea on 7 July 2013 and medium-range forecasts during the period of July 2013 using a global atmospheric model to examine the sensitivity to conversion parameter and evaluate the performance. The revised precipitation production process in the scheme tends to reduce the amount of precipitation, especially in the category of heavy rainfall due to the inefficient conversion of cloud condensate to convective precipitation at colder temperatures. It is also found that the reduced convective heating and drying resulting from suppressed convection and the cooling and moistening due to enhanced detrainment at the cloud top considerably alleviate the warm and dry bias above the lower troposphere over East Asia. A statistical evaluation of the medium-range forecasts demonstrates an overall improvement of the forecast skill in precipitation and large-scale fields. In particular, the revised precipitation conversion parameter significantly improves precipitation forecasts by alleviating the systematic bias of excessive

TABLE 3. RMSEs for forecasts of the 200-, 500- and 850-hPa wind vector ($m\,s^{-1}$), temperature (K), and geopotential height (m) in the Northern Hemisphere (NH; 20°–90°N), tropics (TR; 20°S–20°N), and Southern Hemisphere (SH; 20°–90°S) against the NCEP GFS FNL analysis data for forecast day 5 during the period of July 2013 from CTL. The values in parentheses are those from EXP. A lower RMSE is marked in bold.

	Wind			Temperature			Geopotential height		
	NH	TR	SH	NH	TR	SH	NH	TR	SH
250 hPa	13.66 (**13.33**)	9.89 (**9.74**)	15.80 (**15.67**)	3.00 (**2.88**)	**2.15** (2.20)	2.87 (**2.84**)	59.67 (**57.39**)	21.98 (**20.35**)	83.92 (**83.33**)
500 hPa	8.06 (**7.84**)	**5.78** (5.79)	**11.87** (11.96)	2.00 (**1.96**)	1.39 (**1.27**)	2.87 (**2.85**)	39.56 (**37.90**)	17.56 (**15.63**)	65.49 (**65.45**)
850 hPa	6.20 (**5.99**)	5.13 (**5.05**)	**8.99** (9.07)	2.56 (**2.48**)	1.66 (**1.58**)	3.53 (**3.52**)	30.32 (**28.61**)	15.82 (**15.00**)	52.56 (**52.34**)

precipitation in the original scheme, but it tends to reduce heavy precipitation too much. This underestimation of heavy precipitation can be improved by adjusting the constants in the formulation of the revised conversion parameter [i.e., a and b in Eq. (3)] that control its magnitude. For instance, the reduction of b in Eq. (3a) would increase the convective precipitation. The parameter will be further updated in future work, for example, by using observation or cloud-resolving simulation results with different types of convective storms. The modification used in this study is empirical, although it is based on a cloud-resolving simulation of a convective storm. Further elaboration using a more comprehensive test bed is needed by including the aerosol-aware function, as in the study of Lim (2011). It is apparent from this study that an adequate representation of cloud microphysical processes in a CPS is a crucial factor contributing to the improvement of the forecast skill in NWP models, and therefore more efforts should be made to improve convective microphysics parameterization.

Acknowledgments. The authors are grateful to the editor and three anonymous reviewers for providing valuable comments on this work. The first and second authors were supported by the R&D project on the development of global numerical weather prediction systems of the Korea Institute of Atmospheric Prediction Systems (KIAPS) funded by the Korea Meteorological Administration (KMA). The authors would like to acknowledge the support of the KIAPS Forecasts Verification team. The Pacific Northwest National Laboratory is operated for DOE by Battelle Memorial Institute under Contract DE-AC05-76RLO 1830.

REFERENCES

Arakawa, A., and W. H. Schubert, 1974: Interaction of a cumulus cloud ensemble with the large-scale environment, Part I. *J. Atmos. Sci.*, **31**, 674–701, doi:10.1175/1520-0469(1974)031<0674:IOACCE>2.0.CO;2.

Boyle, J. S., S. A. Klein, D. D. Lucas, H.-Y. Ma, J. Tannahill, and S. Xie, 2015: The parametric sensitivity of CAM5's MJO. *J. Geophys. Res. Atmos.*, **120**, 1424–1444, doi:10.1002/2014JD022507.

Braham, R. R., 1968: Meteorological bases for precipitation development. *Bull. Amer. Meteor. Soc.*, **49**, 343–353.

Chun, H.-Y., and J.-J. Baik, 1998: Momentum flux by thermally induced internal gravity waves and its approximation for large-scale models. *J. Atmos. Sci.*, **55**, 3299–3310, doi:10.1175/1520-0469(1998)055<3299:MFBTII>2.0.CO;2.

Ek, M. B., K. E. Mitchell, Y. Lin, E. Rogers, P. Grunmann, V. Koren, G. Gayno, and J. D. Tarpley, 2003: Implementation of Noah land surface model advances in the National Centers for Environmental Prediction operational mesoscale Eta model. *J. Geophys. Res.*, **108**, 8851, doi:10.1029/2002JD003296.

Emanuel, K. A., 1991: A scheme for representing cumulus convection in large-scale models. *J. Atmos. Sci.*, **48**, 2313–2335, doi:10.1175/1520-0469(1991)048<2313:ASFRCC>2.0.CO;2.

——, and M. Živković-Rothman, 1999: Development and evaluation of a convection scheme for use in climate models. *J. Atmos. Sci.*, **56**, 1766–1782, doi:10.1175/1520-0469(1999)056<1766:DAEOAC>2.0.CO;2.

Fletcher, N. H., 1962: *The Physics of Rain Clouds.* Cambridge University Press, 390 pp.

Grell, G. A., 1993: Prognostic evaluation of assumptions used by cumulus parameterizations. *Mon. Wea. Rev.*, **121**, 764–787, doi:10.1175/1520-0493(1993)121<0764:PEOAUB>2.0.CO;2.

Ham, S., S.-Y. Hong, Y.-H. Byun, and J. Kim, 2009: Effects of precipitation physics algorithms on a simulated climate in a general circulation model. *J. Atmos. Sol.-Terr. Phys.*, **71**, 1924–1934, doi:10.1016/j.jastp.2009.08.001.

Han, J., and H.-L. Pan, 2011: Revision of convection and vertical diffusion schemes in the NCEP Global Forecast System. *Wea. Forecasting*, **26**, 520–533, doi:10.1175/WAF-D-10-05038.1.

Hong, S.-Y., 2010: A new stable boundary-layer mixing scheme and its impact on the simulated East Asian summer monsoon. *Quart. J. Roy. Meteor. Soc.*, **136**, 1481–1496, doi:10.1002/qj.665.

——, and H.-L. Pan, 1998: Convective trigger function for a mass flux cumulus parameterization scheme. *Mon. Wea. Rev.*, **126**, 2599–2620, doi:10.1175/1520-0493(1998)126<2599:CTFFAM>2.0.CO;2.

——, H.-M. H. Juang, and Q. Zhao, 1998: Implementation of prognostic cloud scheme for a regional spectral model. *Wea. Mon. Rev.*, **126**, 2621–2639, doi:10.1175/1520-0493(1998)126<2621:IOPCSF>2.0.CO;2.

——, J. Dudhia, and S.-H. Chen, 2004: A revised approach to ice microphysical processes for the bulk parameterization of clouds and precipitation. *Mon. Wea. Rev.*, **132**, 103–120, doi:10.1175/1520-0493(2004)132<0103:ARATIM>2.0.CO;2.

——, Y. Noh, and J. Dudhia, 2006: A new vertical diffusion package with an explicit treatment of entrainment processes. *Mon. Wea. Rev.*, **134**, 2318–2341, doi:10.1175/MWR3199.1.

——, J. Jang, H. H. Shin, and J. Lee, 2012: An explicitly-coupled shallow convection parameterization with planetary boundary processes. Preprints, *12th WRF Workshop*, Boulder, CO, NCAR, P50. [Available online at http://www2.mmm.ucar.edu/wrf/users/workshops/WS2012/abstracts/p50.htm.]

——, and Coauthors, 2013: The Global/Regional Integrated Model System (GRIMs). *Asia-Pac. J. Atmos. Sci.*, **49**, 219–243, doi:10.1007/s13143-013-0023-0.

Iacono, M.-J., J. S. Delamere, E. J. Mlawer, M. W. Shepherd, S. A. Clough, and W. D. Collins, 2008: Radiative forcing by long-lived greenhouse gases: Calculation with the AER radiative transfer models. *J. Geophys. Res.*, **113**, D13103, doi:10.1029/2008JD009944.

Kim, E.-J., and S.-Y. Hong, 2010: Impact of air-sea interaction on East Asian summer monsoon climate in WRF. *J. Geophys. Res.*, **115**, D19118, doi:10.1029/2009JD013253.

Kim, Y.-J., and A. Arakawa, 1995: Improvement of orographic gravity wave parameterization using a mesoscale gravity wave model. *J. Atmos. Sci.*, **52**, 1875–1902, doi:10.1175/1520-0469(1995)052<1875:IOOGWP>2.0.CO;2.

Lim, K.-S. S., 2011: Investigation of aerosol indirect effects on simulated moist convections. Ph.D. dissertation, Yonsei University, Seoul, South Korea, 186 pp.

——, and S.-Y. Hong, 2012: Investigation of aerosol indirect effects on simulated flash-flood heavy rainfall over Korea. *Meteor. Atmos. Phys.*, **118**, 199–214, doi:10.1007/s00703-012-0216-6.

——, ——, J.-H. Yoon, and J. Han, 2014: Simulation of the summer monsoon rainfall over East Asia using the NCEP GFS cumulus parameterization at different horizontal resolutions. *Wea. Forecasting*, **29**, 1143–1154, doi:10.1175/WAF-D-13-00143.1.

Lord, S. J., 1978: Development and observational verification of a cumulus cloud parameterization. Ph.D. dissertation, University of California, Los Angeles, Los Angeles, CA, 359 pp.

Nober, F. J., H.-F. Graf, and D. Rosenfeld, 2003: Sensitivity of the global circulation to the suppression of precipitation by anthropogenic aerosols. *Global Planet. Change*, **37**, 57–80, doi:10.1016/S0921-8181(02)00191-1.

Pan, H. L., and W.-S. Wu, 1995: Implementing a mass flux convective parameterization package for the NMC Medium-Range Forecast Model. NMC Office Note 409, 40 pp.

Park, H., and S.-Y. Hong, 2007: An evaluation of a mass-flux cumulus parameterization scheme in the KMA global forecast system. *J. Meteor. Soc. Japan*, **85**, 151–169, doi:10.2151/jmsj.85.151.

Rogers, R. R., and M. K. Yau, 1988: *A Short Course in Cloud Physics.* 3rd ed. Pergamon Press, 293 pp.

Segele, Z. T., L. M. Leslie, and P. J. Lamb, 2009: Evaluation and adaption of a regional climate model for the Horn of Africa: Rainfall climatology and interannual variability. *Int. J. Climatol.*, **29**, 47–65, doi:10.1002/joc.1681.

Song, X., G. J. Zhang, and J.-L. F. Li, 2012: Evaluation of microphysics parameterization for convective clouds in the NCAR Community Atmosphere Model CAM5. *J. Climate*, **25**, 8568–8590, doi:10.1175/JCLI-D-11-00563.1.

Tiedtke, M., 1989: A comprehensive mass flux scheme for cumulus parameterization in large-scale models. *Mon. Wea. Rev.*, **117**, 1779–1800, doi:10.1175/1520-0493(1989)117<1779:ACMFSF>2.0.CO;2.

Yang, B., and Coauthors, 2013: Uncertainty quantification and parameter tuning in the CAM5 Zhang–McFarlane convection scheme and impact of improved convection on the global circulation and climate. *J. Geophys. Res. Atmos.*, **118**, 395–415, doi:10.1029/2012JD018213.

Zhang, G. J., and N. A. McFarlane, 1995: Sensitivity of climate simulations to the parameterization of cumulus convection in the Canadian Climate Centre general circulation model. *Atmos.–Ocean*, **33**, 407–446, doi:10.1080/07055900.1995.9649539.